Fuel 108 (2013) 430–438

Contents lists available at SciVerse ScienceDirect

Fuel

journal homepage: www.elsevier.com/locate/fuel

Effect of catalytic site position: Nickel nanocatalyst selectively loaded inside or outside carbon nanotubes for methane dry reforming

Qingxiang Ma [a,b], Ding Wang [a], Mingbo Wu [c], Tiansheng Zhao [b], Yoshiharu Yoneyama [a], Noritatsu Tsubaki [a,d,*]

[a] Department of Applied Chemistry, School of Engineering, University of Toyama, Gofuku 3190, Toyama 930-8555, Japan
[b] State Key Laboratory Cultivation Base of Natural Gas Conversion, Ningxia University, Yinchuan 750021, China
[c] State Key Laboratory of Heavy Oil Processing, China University of Petroleum, Qingdao 66555, China
[d] JST, ACT-C, Tokyo 102-8666, Japan

HIGHLIGHTS

- Ni nanoparticles were selectively loaded inside or outside CNTs.
- Ni inside CNTs showed higher activity than Ni outside CNTs for methane dry reforming.
- Ni inside CNTs was more stable than Ni outside CNTs for methane dry reforming.
- Enhanced catalytic performance was attributed to the confinement of CNTs channels.

GRAPHICAL ABSTRACT

The catalysts with nickel nanoparticles selectively loaded inside or outside CNTs were prepared via wet chemical method and the catalytic performance was studied to clarify the different catalytic site position effect for methane dry reforming. The reaction results showed that I–Ni/CNTs had higher catalytic activity and better stability than O–Ni/CNTs.

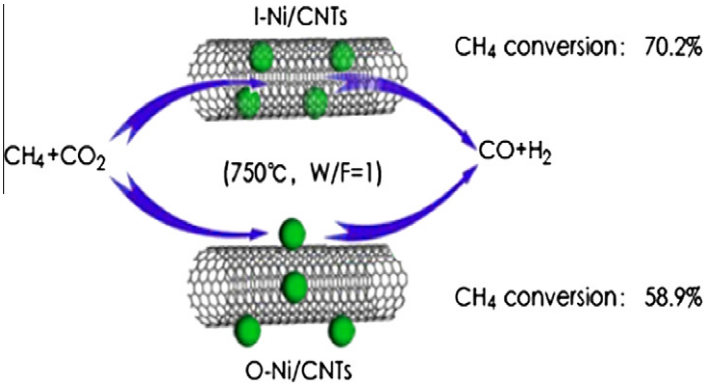

ARTICLE INFO

Article history:
Received 20 September 2012
Received in revised form 2 December 2012
Accepted 4 December 2012
Available online 22 December 2012

Keywords:
Methane dry reforming
Carbon nanotubes
Nickel-based catalyst
Catalytic site position
Confinement effect

ABSTRACT

The catalysts with nickel nanoparticles selectively loaded inside or outside carbon nanotubes (CNTs) were prepared via wet chemical method to study the different catalytic site position effect such as inside and outside CNTs. The catalysts were characterized by N_2 adsorption, transmission electron micrographs (TEM), X-ray diffraction (XRD), H_2-temperature programmed reduction (H_2-TPR), X-ray photoelectron spectroscopy (XPS) and Raman spectroscopy. TEM images and XPS demonstrated that most of nickel nanoparticles were controlled to be loaded at interior or exterior surface of CNTs. The H_2-TPR analysis results showed that the nickel oxide at the inside of the CNTs was easier to be reduced by H_2, which was attributed to the confinement effect of CNTs. Furthermore, this different reducibility resulted in an obvious different catalytic performance in terms of methane reforming of carbon dioxide. The reaction results demonstrated that the nickel catalyst with the nanoparticles inside CNTs exhibited higher catalytic activity and stability compared with the catalyst where nickel nanoparticles loaded outside CNTs.

* Corresponding author at: Department of Applied Chemistry, School of Engineering, University of Toyama, Gofuku 3190, Toyama 930-8555, Japan. Tel./fax: +81 76 445 6846.
E-mail address: tsubaki@eng.u-toyama.ac.jp (N. Tsubaki).

0016-2361/$ - see front matter © 2012 Elsevier Ltd. All rights reserved.
http://dx.doi.org/10.1016/j.fuel.2012.12.028

1. Introduction

Methane dry reforming has received significant attention in recently years, as the process of converted two greenhouse gases CH_4 and CO_2 to valuable syngas. The reaction equation is showed as following:

$$CH_4 + CO_2 \rightarrow 2CO + 2H_2 \quad (1)$$

The dry reforming reaction is accompanied by several side reactions, such as the reverse water–gas shift reaction (2), the methane cracking reaction (3) and the Boudouard reaction (4) [1].

$$CO_2 + H_2 \rightarrow H_2O + CO \quad (2)$$

$$CH_4 \rightarrow C + 2H_2 \quad (3)$$

$$2CO \rightarrow CO_2 + C \quad (4)$$

Compared to steam reforming of CH_4 or partial oxidation of CH_4 process, dry reforming of CH_4 has advantages in industrial demand for the production of syngas with H_2/CO ratio close to 1/1, which is more suitable for further synthesis of liquid hydrocarbon in Fischer–Tropsch synthesis on Fe-based catalyst and dimethyl ether (DME). Meanwhile, the dry reforming of methane was considered as one of the best way to store and transport solar or atomic energy.

In the previous reports, many VIII metals, such as Co, Ni, Rh, Ru and Pt, loaded on different supports have been used as catalyst for dry reforming reaction [2–9]. Nickel-based catalysts are more interesting than noble metal catalysts due to higher availability and lower price.

Recently, great attention has been paid to carbon materials with novel nanostructure such as carbon nanotubes, carbon nanofibers and carbon spheres. CNTs have unique properties such as large surface areas, mesopore structures, and uniform pore size distribution, resistance to high temperature, acid or base [10]. As a novel support material, CNTs were widely used as support material for catalytic reaction such as Fischer–Tropsch synthesis [11,12], higher alcohol synthesis [13,14], methanol synthesis [15], selective hydrogenation [16] and ammonia synthesis [17]. First-principles study revealed that deviation of the graphene layer from planarity caused π-electron density to shift from the concave inner surface to the convex outer surface, leading to an electron-deficient interior surface and an electron-enrich exterior surface. Furthermore, the different electronic properties between interior and the exterior CNTs lead to different catalytic performance when the catalyst was selectively loaded inside or outside CNTs [18]. Bao and Dalai compared the difference of catalytic site position between the interior and the exterior of the CNTs in Fischer–Tropsch synthesis [19,20]. They found that the catalyst filled inside CNTs presented lower reduction temperature than loaded outside CNTs, which was attributed to the different electronic properties of the inner and outer surface of the CNTs. According to their reports, the metal- support interaction inside CNTs channels may be different from that on the exterior surface of CNTs, which determined the difference catalytic performance.

In this report, the catalysts with nickel nanoparticles loaded inside or outside CNTs were prepared through wet chemical method, used for CO_2 reforming of CH_4, and the effects of catalytic sites position at interior or exterior surface of CNTs were investigated. TEM, BET, XRD, XPS, H_2-TPR, TG and Raman spectroscopy were employed to characterize the physicochemical property of the catalysts and the spent catalysts.

2. Experimental

2.1. Catalyst preparation

Raw multi-wall carbon nanotubes (inner diameter: 4–10 nm, Chengdu, China) (denoted as raw CNTs) were firstly refluxed in concentrated HNO_3 (65 wt.%) at 120 °C for 14 h, and then washed with deionized water until pH = 7. The sample was dried at 120 °C overnight (denoted as acid-treated CNTs). And then the obtained sample was further calcined at 900 °C under Ar atmosphere for 3 h (denoted as heat-treated CNTs). For the preparation of catalysts with Ni particles inside CNTs, catalyst was prepared by an improved wetness impregnation method. A certain amount of $Ni(NO_3)_2$ were dissolved in the ethanol solvent. Above treated CNTs with open ends was impregnated with the nickel solution and then vacuumed for 0.5 h. After ultrasonic treatment for 0.5 h, the sample was impregnated with deionized water and dried at 60 °C overnight. By this method, the particles could be easily deposited inside CNTs (denoted as I–Ni/CNTs). In order to prepare the catalyst with Ni catalytic site on the exterior surface of nanotubes, dimethyl benzene was used to fill the pore of nanotubes. The volume of the solvent was equal to the pore volume of CNTs. Then the nickel nitrate solution was added to the pore-filled support. After ultrasonic treatment for 0.5 h, the sample was dried at 60 °C overnight (denoted as O–Ni/CNTs). For the comparison of catalytic activity with the Ni/CNTs, the Ni/AC (active carbon) catalyst was prepared by wet impregnation method. A specified amount of $Ni(NO_3)_2$ was dissolved in deionized water. The amount of solution was equal to total volume of AC. Subsequently, the impregnated Ni/AC sample was treated by ultrasonic for 0.5 h and dried at 60 °C overnight.

All the samples were calcined in Ar at 450 °C for 3 h. Before the reaction, the catalyst was reduced at 500 °C for 2 h under a flow of 5% hydrogen of 40 ml/min. The loading of Ni for all catalysts was 10.0 wt.%.

2.2. Catalyst characterization

Nitrogen adsorption measurements were carried out at −196 °C under a Quantachrome Instruments AUTOSORB-1, and BET surface area and the pore size distribution were determined from the isotherms. The samples were outgassed at 200 °C for 2 h before each test. The samples were characterized by H_2 temperature programmed reduction (H_2-TPR) using BELCAT-B-TT (BEL.JAPAN INC.) in a flow system using 5% H_2/Ar mixture gases with 10 °C/min temperature ramp and with a flow rate of 30 mL/min. The power X-ray diffraction patterns were measured using Rigaku Corporation Instruments RinT2200 V/PC with monochromatized Cu/Kα radiation. High resolution transmission electron micrographs (HRTEM) were obtained with a JEOL JEM-2100 UHR transmission electron microscope operated at 200 kV. Raman spectra were recorded with a Raman spectrometer using a laser excitation line at 514.5 nm. X-ray photoelectron spectroscopy (XPS) study was conducted using ESCALAB 250Xi spectrometer equipped with a monochromatized Al Kα source focused to a spot size of 0.2 mm. The position of the C 1s peak (284.5 eV) was used to correct the binding energies for all catalysts for possible charging effects. The carbon deposition was characterized by thermogravimetric analysis using Shimadzu DTG-60 instrument. The spent catalyst was heated in a platinum sample cell in the air atmosphere from room temperature to 750 °C at a ramp rate of 10 °C/min.

2.3. Catalytic reaction

Dry reforming experiments were carried out in fixed-bed quartz reactor (6 mm i.d.) under atmospheric pressure. A reactant gas

stream that consisted of CH_4, CO_2 and Ar with a molar ratio of 4.5:4.5:1 was used. The *W*/*F* was fixed at 1 g h/mol. The effluent gases being cooled through an ice trap were analyzed with two gas chromatographs. CO, CO_2 and CH_4 were analyzed by Shimadzu GC-8A with a Porapak Q column and a thermal conductivity detector (TCD). H_2 was analyzed by GC-320 (GL Science Co.) with an activated carbon column and a TCD. The conversions of CO_2, CH_4 and the H_2/CO molar ratio were calculated as following equations:

$$C_{CO2}\% = [CO_{2\,in} - CO_{2\,out}]/CO_{2\,in}$$

$$C_{CH4}\% = [CH_{4\,in} - CH_{4\,out}]/CH_{4\,in}$$

$$H_2/CO \text{ molar ratio} = H_{2out}/CO_{out}$$

3. Results and discussion

3.1. Catalyst characterizations

3.1.1. TEM analysis

TEM was employed to study the morphology of the CNTs supports and CNTs based catalysts. Fig. 1 shows the TEM images of raw CNTs and the CNTs after nitrate acid treatment. For the raw CNTs, it can be seen that CNTs are curved and most of ends are closed. After nitrate acid treatment, most of ends are open. The heat-treated CNTs and the location of nickel nanoparticles on heat-treated CNTs can be further verified by HRTEM images. Fig. 2 shows the HRTEM images and the particle size distributions of O–Ni/CNTs catalyst and I–Ni/CNTs catalyst. For the O–Ni/CNTs catalyst, it clearly shows that most of nickel nanoparticles are loaded outside of CNTs with uniform dispersion. Statistics shows that more than 80% of nickel nanoparticles load on the exterior surface of CNTs. Ni nanoparticles loaded purely outside of CNTs is attributed to that dimethyl benzene was filled in the CNTs channels by the first step. The dimethyl benzene in the CNTs channels hindered the Ni salt solution entering into the CNTs channels. As shown in the Fig. 2b, most of nickel nanoparticles have the size within the range of 5–11 nm, the average size of nickel nanoparticles is 7.87 nm. For the I–Ni/CNTs catalyst, due to the relatively low surface tension of the ethanol used as the solvent, an equal amount of $Ni(NO_3)_2$ solution was almost entirely sucked into channels of CNTs by the capillary force. It can be observed that more than 80% nickel particles filled inside the CNTs channel and most of nickel particles have the size in the range of 5–10 nm with the

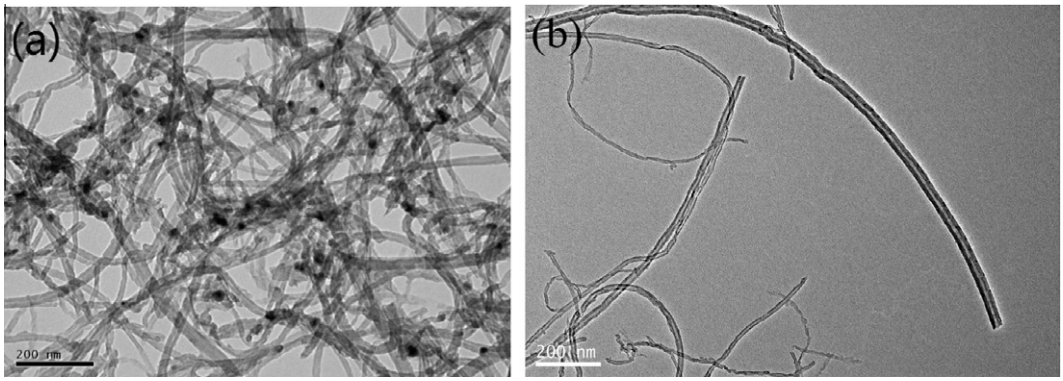

Fig. 1. TEM images of (a) raw CNTs and (b) acid-treated CNTs.

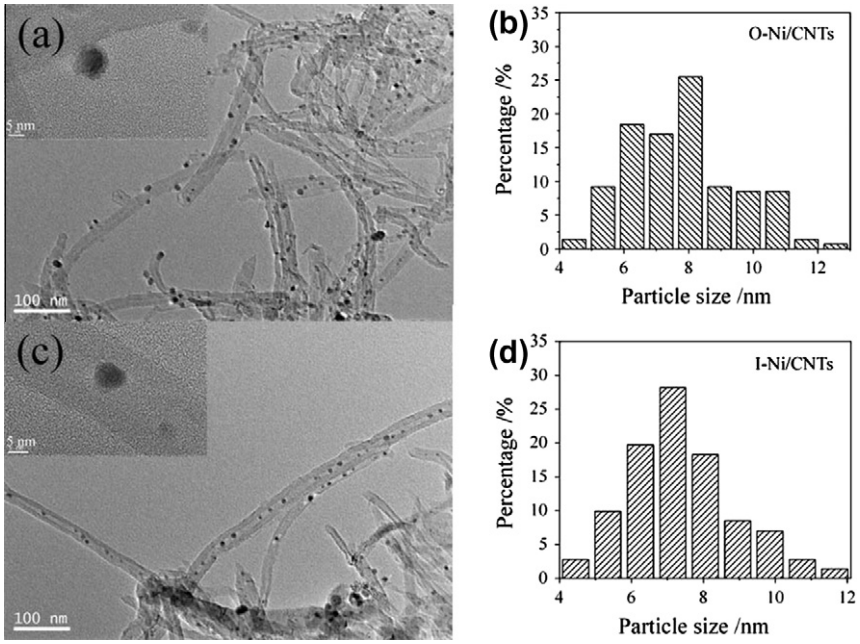

Fig. 2. TEM images (a,c) and particles size distribution (b,d) of O-Ni/CNTs and I–Ni/CNTs.

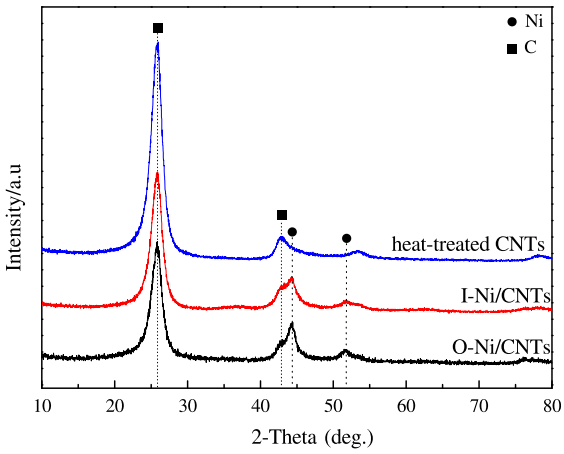

Fig. 3. XRD patterns of O-Ni/CNTs and I–Ni/CNTs catalyst before reduction.

average value about 7.43 nm. It is indicated that there is no significant difference for the nanoparticles size between O–Ni/CNTs and I–Ni/CNTs.

3.1.2. XRD analysis

The phase of the CNTs and CNTs based catalysts was analyzed by XRD. XRD patterns of the heat-treated CNTs support and the nickel loaded inside or outside CNTs catalysts are shown in Fig. 3. The peaks at 26.2° and 42.5° are the characteristic peaks of CNTs which correspond to graphite layers of multiwall carbon nanotubes. This indicates that after treatment with acid and calcination at high temperature, the graphitic structure is still kept. The other peaks at 44.3°and 51.8° in the XRD patterns are assigned to the (111) and (200) crystallographic plane of Ni, respectively. Comparing with the intensities of the peaks, the O–Ni/CNTs is a little higher than I–Ni/CNTs. Based on the line width of the (111) diffraction plane, the crystallite particles size of Ni is determined using Scherrer's equation. The Ni particle size of O–Ni/CNTs and I–Ni/CNTs is 7.5 ± 1.1 nm and 7.1 ± 1.7 nm, respectively, suggesting that the particle size of these two samples is almost equal.

3.1.3. Nitrogen adsorption–desorption analysis

The N_2 adsorption–desorption isotherms were used to determine the pore structure of the catalysts. The N_2 adsorption–desorption isotherms and the corresponding pore size distribution of the CNTs and CNTs supported catalysts are shown in Fig. 4, respectively. All the samples exhibit typical type-IV adsorption isotherms with clear H3 hysteresis loops at higher relative pressure, suggesting that mesopores appear in the samples [21]. After heat treatment at 900 °C in Ar atmosphere, the amount of N_2 adsorbed on the sample near $P/P_0 = 1$ decrease, indicating the decreasing of large mesopores and macopores of the samples. Compared with that of heat-treated CNTs, the N_2 adsorption quantity of Ni/CNTs near the $P/P_0 = 1$ increase, it is attributed to the increasing of accumulated pores. The hysteresis loops appearing at medium relative pressure range of 0.4–0.8 and higher relative pressure are associated with the capillary condensation in small mesopores and accumulated pore, respectively [22]. Compared with that of O–Ni/CNTs, the hysteresis loop of I–Ni/CNTs almost disappear in the adsorption–desorption isotherms curve, because of the fact that most of channels of CNTs are loaded with Ni particles which decrease the pore size of CNTs. Table 1 shows the nitrogen adsorption measurement data of the support and the catalysts. It can be seen that the BET surface area increases from 173 to 224 m^2/g and the pore volume decreases from 1.56 to 0.89 cm^3/g after nitrate acid treatment. This illustrates that treatment of CNTs with nitric acid open the ends of CNTs and expose their internal surface area. The increasing micropore volume and decreased mesopore volume after acid treatment suggest some defects formed on the CNTs walls. After loading the Ni particles, the mesopore volume of the I–Ni/CNTs is lower than that of O–Ni/CNTs, because most channels of CNTs are filled with Ni nanoparticles.

The pore size distributions of CNTs and the catalysts are shown in Fig. 4b. The pore size distribution curves indicate that there are two types of pores, which are considered as inner pore and aggregated pore [22]. It is obvious that the small mesopore of 3–5 nm is the inner pore of CNTs and the larger pore corresponds to the aggregated pore. It can be seen that the size of small mesopore is clearly increased after heat treatment. In contrast, the size of small mesopore of nickel catalyst is decreased, which is attributed to the nickel particles filled inside channels or the ends of CNTs.

3.1.4. XPS analysis

The electronic states of the nickel catalysts were studied by using X-ray photoelectron spectroscopy (XPS). Fig. 5 shows the XPS spectra of I–Ni/CNTs and O–Ni/CNTs. The Ni2p spectral region for all samples shows peak at 853.1–853.3 eV, which is characteristic of Ni^0. The peak at 856.4 ± 0.2 eV with satellite around 860.8 eV is due to the presence of NiO. Meanwhile, it should be noted that the intensity of the Ni2p peaks from O–Ni/CNTs is much higher than that from I–Ni/CNTs although the nickel loading is similar. It is considered that the walls of CNTs have a shielding effect, which leads to a significantly attenuation of Ni2p signal in I–Ni/CNTs. The XPS results also prove that the vast majority of nickel particles are loaded inside the channels of CNTs of I–Ni/CNTs. This is well in accordance with the HRTEM results.

3.1.5. Raman spectra

Raman spectroscopy was employed to analyze the degree of graphitization of CNTs [23,24]. Fig. 6 shows the Raman spectra of I–Ni/CNTs, O–Ni/CNTs and support CNTs which were measured with 514.5 nm excitation over the Raman shift interval of 1000–2000 cm^{-1}. Two prime intense Raman bands correspond to the *D*-bands and *G*-bands, respectively. The *D*-band at ~1342 cm^{-1} is related to the defects and disorders of structures in carbon materials. The *G*-band is an intrinsic feature of carbon nanotubes that is closely related to vibrations in all sp^2 carbon materials. The *G*-bands of nanotubes are known to consist of two main components, G^+ and G^-. This band shows two different components [25]. The lower frequency component is associated with vibrations along the circumferential direction (G^+), and the higher frequency component (G^-) is attributed to vibrations along the direction of the nanotubes axis [26]. The I_D/I_G^+ (denoted as *R*) value represents the degree of disorder in graphite layer. The *R* values for samples are 1.06 (acid treated CNTs), 1.31 (heat-treated CNTs), 1.36 (O–Ni/CNTs) and 1.50 (I–Ni/CNTs), respectively. It is obvious that the *R* value is increased after heating treatment, indicating that heat treatment made the CNTs disordered. Furthermore, the *R* value of O–Ni/CNTs, loading Ni outside the CNTs support, only increases from 1.31 to 1.36. But for I–Ni/CNTs prepared by loading Ni inside of CNTs, its *R* value increased more obviously from 1.31 to 1.50. It is indicated that nickel nanoparticles loading outside CNTs almost had no effect on the graphite layer of CNTs. Meanwhile, the O–Ni/CNTs had better ordered structure of the graphite sheets than the I–Ni/CNTs, suggesting the higher level disorder and defect in the case of CNTs with nickel filled inside of CNTs. This phenomenon is also observed in the HRTEM results above.

3.1.6. H_2-TPR analysis

The reducibility of the catalysts is a crucial factor influencing its catalytic performance. The H_2-TPR patterns of nickel catalyst loaded inside or outside CNTs before reduction and the bulk NiO

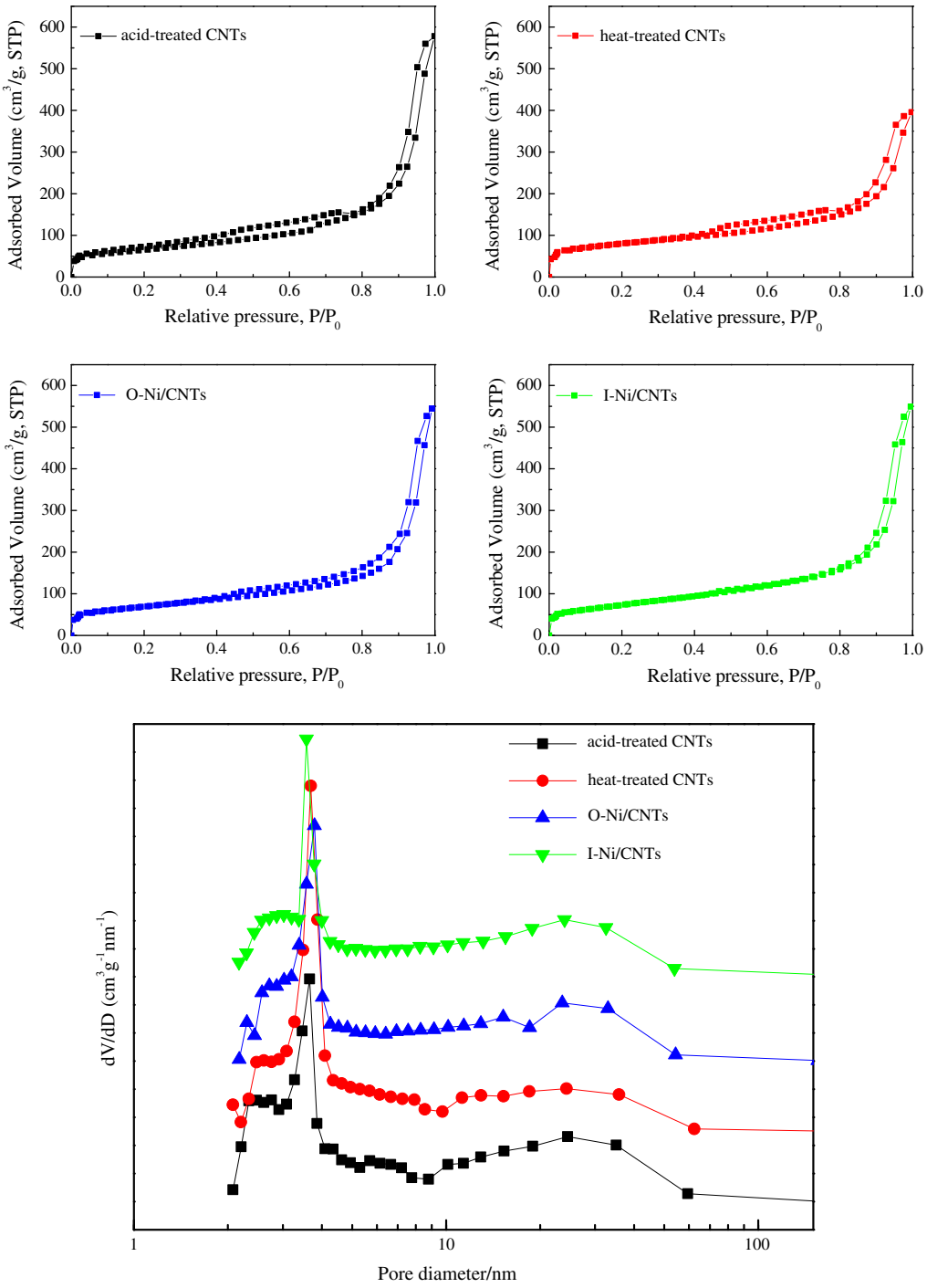

Fig. 4. N_2 adsorption–desorption isotherms and pore distribution of acid-treated CNTs, heat-treated CNTs, O-Ni/CNTs and I–Ni/CNTs.

Table 1
Surface property of fresh, pre-treated CNTs and nickel catalysts.

Catalyst	BET surface area[a] (m^2/g)	V_{Total}[b] (cm^3/g)	V_{Micro}[c] (cm^3/g)	V_{Meso}[d] (cm^3/g)
Raw CNTs	173	1.56	0.07	1.49
Acid-treated CNTs	224	0.89	0.10	0.79
Heat-treated CNTs	265	0.61	0.12	0.49
I–Ni/CNTs	260	0.84	0.11	0.73
O–Ni/CNTs	249	0.85	0.10	0.75

[a] The surface area was determined by N_2 adsorption.
[b] V_{Total}: Total pore volume was estimated at a relative pressure $P/P_0 = 0.99$.
[c] V_{Micro}: Micropore volume was determined from the Dubinine Radushkevic (DR) equation.
[d] V_{Meso}: Mesopore volume was determined from the subtraction of micropore volume from total pore volume.

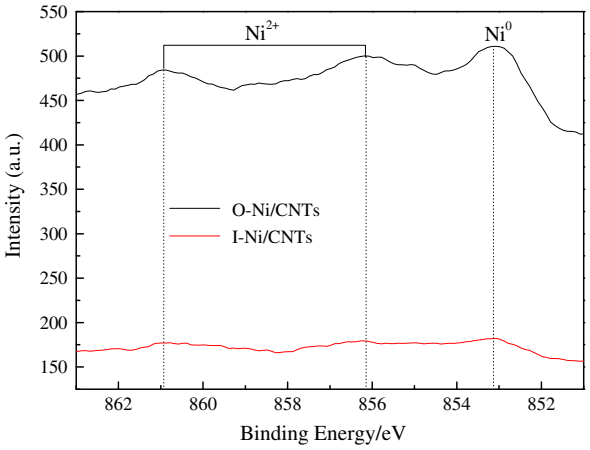

Fig. 5. Ni2p XPS spectra of O-Ni/CNTs and I–Ni/CNTs.

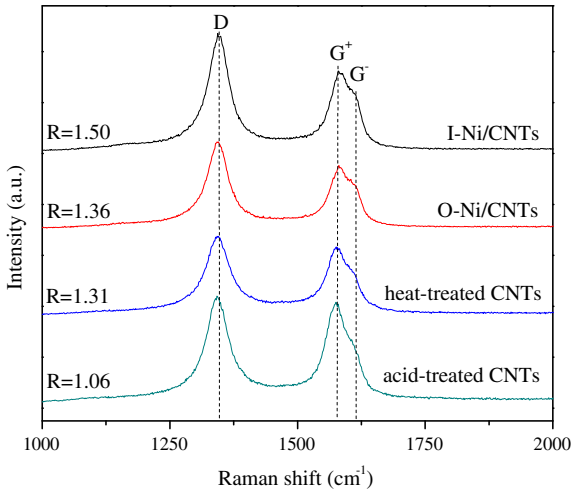

Fig. 6. Raman spectra of acid-treated CNTs, heat-treated CNTs, O-Ni/CNTs and I–Ni/CNTs.

are displayed in Fig. 7. There are two reduction peaks for both catalysts and one peak for the bulk NiO sample. The H_2 reduction peak of bulk NiO appears at 365 °C, higher than those of CNTs supported catalysts. For the catalyst I–Ni/CNTs, a lower reduction peak at 293 °C is assigned to the reduction of NiO particles to metallic nickel inside of CNTs. The other strong peak around 510 °C is associated with a reduction of support CNTs [27]. Compared with that of the I–Ni–CNTs, the reduction peak of O–Ni/CNTs appears at 320 °C, about 30 °C higher than that of I–Ni/CNTs, indicating that NiO particles interacting with the exterior wall are more difficult to be reduced than those with the interior wall. The different reducibility arises from the different electron deficiency of the interior and the exterior surface which leads to weaken the bonding strength of Ni–O and reduce I–Ni/CNTs more easily.

3.2. Catalytic activity

The blank experiment with the unloaded CNTs as catalyst was carried out and the result showed that no conversion of CO_2 or CH_4 was detected. The catalytic performances of Ni loaded inside or outside CNTs are compared in Fig. 8 with the reaction temperature increased from 500 to 800 °C. It is clearly showed that the catalytic activity of Ni/AC is obvious lower than that of CNTs based catalyst, especially at higher temperature. The decreased catalytic

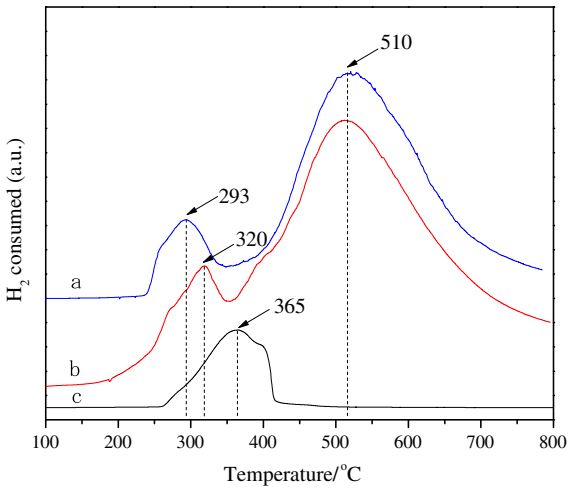

Fig. 7. H_2-TPR profiles of O–Ni/CNTs, I–Ni/CNTs and bulk NiO catalyst before reduction. (a. I–Ni/CNTs, b. O–Ni/CNTs, c. bulk NiO.)

activity might be due to the structure collapse of the activated carbon support. The catalytic performance of CNTs based catalyst is increased with the reaction temperature, indicating that the CNTs are more thermal-stable than activated carbon. When the reaction temperature exceeds 600 °C, the CO_2 conversion is higher than the corresponding CH_4 conversion. The effect of reaction temperature on the ratio of H_2/CO is also shown in Fig. 8c. There was a significant increase in the H_2/CO ratio with the increasing temperature from 700 °C to 800 °C. The lower H_2 production observed at 700 °C indicates that the reverse water–gas shift reaction may also have occurred under these conditions. For comparison of the two CNTs catalysts, higher catalytic activity is clearly observed on I–Ni/CNTs catalyst than on O–Ni/CNTs catalyst. At lower temperature, the catalytic activities of the two catalysts are similar. With the reaction temperature increasing, the catalytic activity of I–Ni/CNTs is higher than that of O–Ni/CNTs. It is considered that nickel nanoparticle deposited inside CNTs has higher catalytic performance than that loaded outside CNTs.

In order to examine the effect of the nickel particles position on the catalytic stability, the catalytic stability evaluation of the catalysts was conducted at 750 °C. The CH_4 and CO_2 conversion at 750 °C and W/F = 1 g h/mol are shown in Fig. 9. The I–Ni/CNTs catalyst shows higher catalytic activity and the conversions of CO_2 and CH_4 are about 70.2% and 83.4%, respectively. The catalytic activity of O–Ni/CNTs catalyst is lower, where the conversions of CO_2 and CH_4 are 58.9% and 75.6%, separately. After 8 h on stream, both catalysts show a slight activity loss in CO_2 and CH_4 conversion. For the I–Ni/CNTs, the CH_4 and CO_2 conversions decrease to 65.4% and 78.8%, respectively. The H_2/CO ratio obtained with the I–Ni/CNTs is higher that of O–Ni/CNTs and all of that decrease with the time on stream. Compared with the I–Ni/CNTs, the O–Ni/CNTs exhibits a lower stability where the conversions of CH_4 and CO_2 only reach 50.1% and 66.1%, respectively. It is clear that Ni particle deposited inside CNTs is more stable for methane dry reforming.

3.3. Characterization of catalysts after reaction

After 8 h reaction, the spent catalysts were subjected to TG treatment under air atmosphere to investigate the carbon deposition. The TG curves are displayed in Fig. 10. As for the TG curve, its general trend is downward as the temperature increased. However, there is a minor rise in the region from 300 to 500 °C; it is because that the oxidation of metallic nickel occurred under air atmosphere. The TG curve indicated that the carbon materials

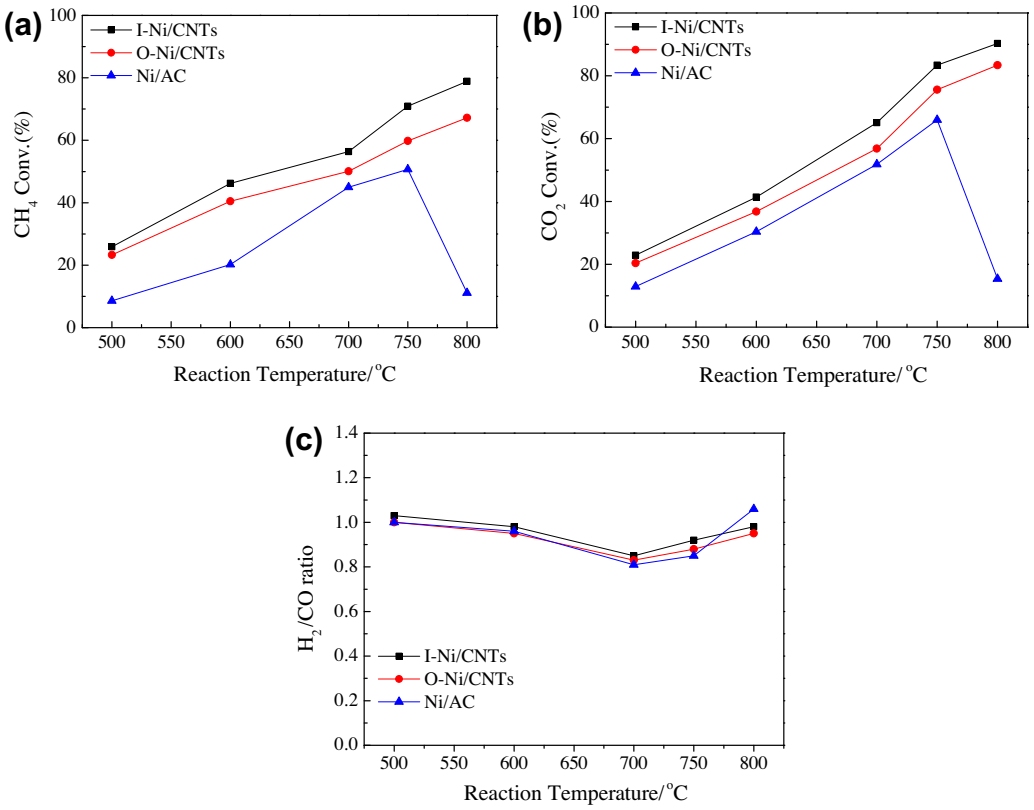

Fig. 8. The conversion–temperature relationships of Ni/AC, O–Ni/CNTs and I–Ni/CNTs catalyst. (a) CH_4 conversion; (b) CO_2 conversion; (c) H_2/CO ratio. (Reaction conditions: W/F = 1 g h/mol.)

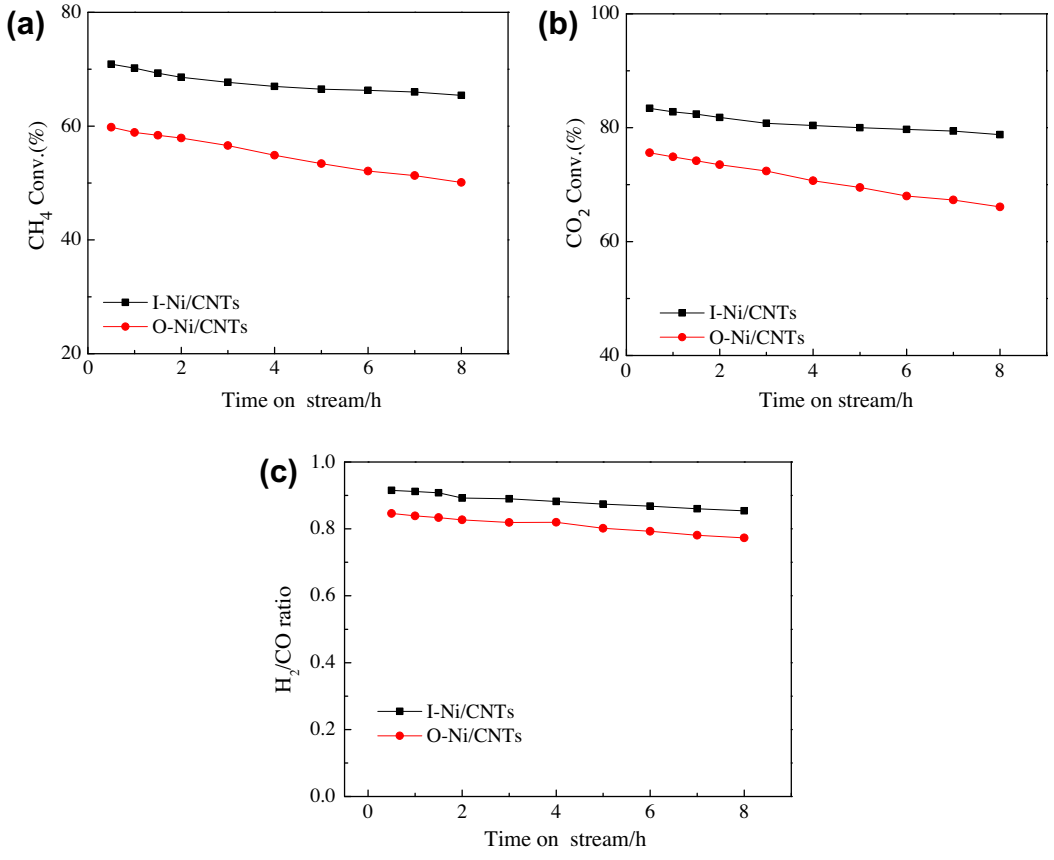

Fig. 9. Catalytic stability of I–Ni/CNTs and O–Ni/CNTs. (a) CH_4 conversion; (b) CO_2 conversion; (c) H_2/CO ratio. (Reaction conditions: 750 °C, W/F = 1 g h/mol.)

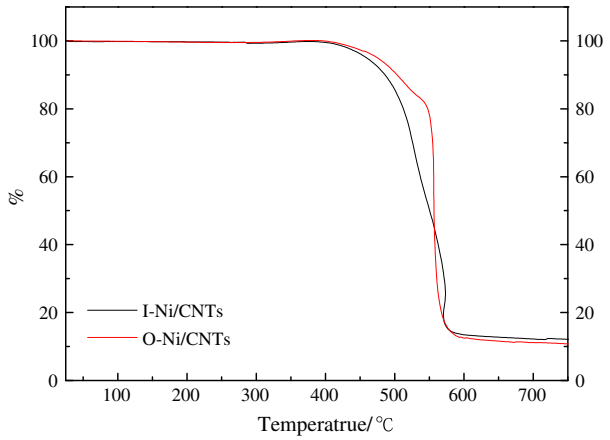

Fig. 10. TG analysis of spent I–Ni/CNTs and O-Ni/CNTs catalysts after the reforming reaction at 750 °C for 8 h.

could be burnt under air atmosphere in the range between 300 °C and 750 °C. At general condition, the weight loss appeared at TG curve represented the carbon deposition of the catalysts. For the CNTs substrates which could also be burnt out at the same conditions, the weight loss could not represent the carbon deposition. But it can be calculated though ternary equation as following:

$$m_{CNTs} + m_{deposited\ carbon} + m_{Ni} = C\ (\text{mass of spent samples for TG analysis}) \quad (5)$$

$$m_{Ni}/(m_{Ni} + m_{CNTs}) = 0.1\,\text{mass of spent sample} \quad (6)$$

$$m_{Ni} = C \times (1 - \text{the percent of weight loss}) \times (M_{Ni}/M_{NiO}) \quad (7)$$

The total carbon deposition of the spent I–Ni/CNTs and O–Ni/CNTs samples were 9.3% and 20.8%, respectively. It is suggested that Ni outside CNTs is easier to form carbon deposition than Ni inside CNTs.

In order to further confirm the morphology of coke of catalysts after 8 h reaction. TEM analysis of the spent catalysts was performed. The TEM images are presented in Fig. 11 for spent I–Ni/CNTs and O–Ni/CNTs samples. It can be seen that the spent samples were still kept carbon nanotubes after the samples were used in methane reforming with CO_2 at 750 °C for 8 h. As shown in Fig. 11a, it is obvious that the Ni particles inside CNTs had size growth large big along the nanotubes direction with a rod-like morphology. It should be the amorphous carbon around Ni particle. Fig. 11b displayed clearly that the Ni particles outside CNTs formed graphite like carbon over spent catalyst.

4. Conclusions

Ni nanoparticles loaded inside or outside CNTs were selectively prepared via wet chemical method. The TEM images and XPS characterization demonstrated that nickel nanoparticles loaded inside or outside CNTs catalysts were obtained as designed. H_2-TPR indicated that the nickel nanoparticles inside the CNTs were easy to be reduced. The effects of catalytic sites position at interior or exterior surface of CNTs on catalytic activity were researched by CO_2 reforming of CH_4. The reaction results showed that the catalytic activity of I–Ni/CNTs was higher than that of O–Ni/CNTs catalyst. Furthermore, the I–Ni/CNTs catalyst also exhibited high stability. All these can be ascribed to the electric density difference between interior and exterior surface of CNTs and the confinement effect of CNTs. The analysis of spent catalysts indicated that amorphous carbon formed on the catalyst with Ni particles inside CNTs channels, while another type of graphite carbon appeared on the catalyst with Ni particles outside CNTs channels.

Acknowledgements

The authors thank for the financial supports of Major Project of Chinese National Programs for Fundamental R & D (2012CB723106) and International Cooperation Project from Chinese Ministry of Science and Technology (2010DFB40440).

References

[1] Castro Luna AE, Iriarte ME. Carbon dioxide reforming of methane over a metal modified Ni–Al_2O_3 catalyst. Appl Catal A 2008;343(1–2):10–5.
[2] Soloviev SO, Kapran AY, Orlyk SN, Gubareni EV. Carbon dioxide reforming of methane on monolithic Ni/Al_2O_3-based catalysts. J Nat Gas Chem 2011;20(2):184–90.
[3] Özkara-Aydınoğlu Ş, Aksoylu AE. Carbon dioxide reforming of methane over Co-X/ZrO_2 catalysts (X = La, Ce, Mn, Mg, K). Catal Commun 2010;11(15):1165–70.
[4] Djinović P, Batista J, Pintar A. Efficient catalytic abatement of greenhouse gases: Methane reforming with CO_2 using a novel and thermally stable Rh–CeO_2 catalyst. Int J Hydrogen Energy 2012;37(3):2699–707.
[5] Paturzo L, Gallucci F, Basile A, Vitulli G, Pertici P. An Ru-based catalytic membrane reactor for dry reforming of methane—its catalytic performance compared with tubular packed bed reactors. Catal Today 2003;82(1–4):57–65.
[6] Nagai M, Nakahira K, Ozawa Y, Namiki Y, Suzuki Y. CO_2 reforming of methane on Rh/Al_2O_3 catalyst. Chem Eng Sci 2007;62(18–20):4998–5000.
[7] Souza MMVM, Aranda DAG, Schmal M. Reforming of methane with carbon dioxide over Pt/ZrO_2/Al_2O_3 catalysts. J Catal 2001;204(2):498–511.
[8] Tao K, Zhang Y, Terao S, Tsubaki N. Development of platinum-based bimodal pore catalyst for CO_2 reforming of CH_4. Catal Today 2010;153(3–4):150–5.
[9] Tao K, Zhang Y, Terao S, Yoneyama Y, Kawabata T, Matsuda K, et al. Chemical and spatial promotional effects of bimodal pore catalysts for methane dry reforming. Chem Eng J 2011;170:258–63.
[10] Ajayan PM. Nanotubes from carbon. Chem Rev 1999;99(7):1787–800.

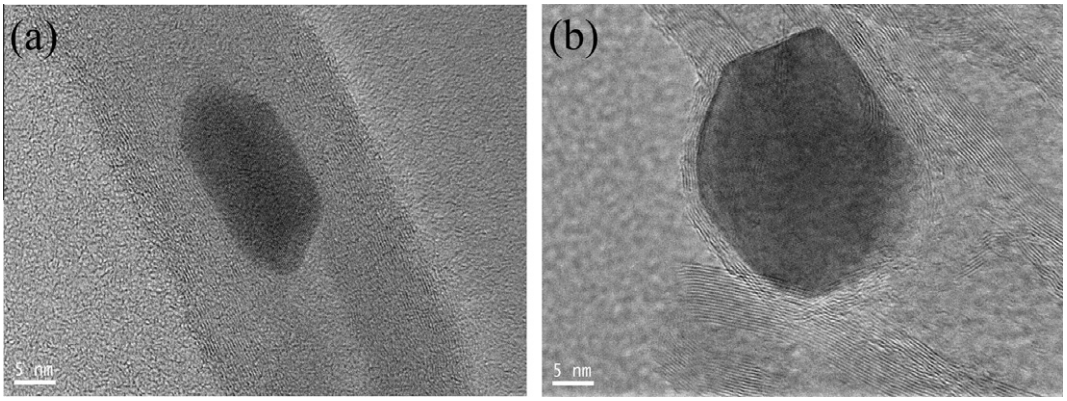

Fig. 11. TEM images of spent (a) I–Ni/CNTs and (b) O-Ni/CNTs catalysts after the reforming reaction at 750 °C for 8 h.

[11] van Steen E, Prinsloo FF. Comparison of preparation methods for carbon nanotubes supported iron Fischer–Tropsch catalysts. Catal Today 2002;71(3–4):327–34.
[12] Bahome MC, Jewell LL, Hildebrandt D, Glasser D, Coville NJ. Fischer–Tropsch synthesis over iron catalysts supported on carbon nanotubes. Appl Catal A 2005;287(1):60–7.
[13] Dong X, Liang X-L, Li H-Y, Lin G-D, Zhang P, Zhang HB. Preparation and characterization of carbon nanotube-promoted Co–Cu catalyst for higher alcohol synthesis from syngas. Catal Today 2009; 147(2):158–65.
[14] Venkateswara Rao Surisetty AT, Dalai AK. Synthesis of higher alcohols from syngas over alkali promoted MoS2 catalysts supported on multi-walled carbon nanotubes.. Appl Catal A 2009;365:243–51.
[15] Liang XL, Dong X, Lin GD, Zhang HB. Carbon nanotube-supported Pd–ZnO catalyst for hydrogenation of CO_2 to methanol. Appl Catal B 2009;88(3–4):315–22.
[16] Antonetti C, Oubenali M, Raspolli Galletti AM, Serp P, Vannucci G. Novel microwave synthesis of ruthenium nanoparticles supported on carbon nanotubes active in the selective hydrogenation of p-chloronitrobenzene to p-chloroaniline. Appl Catal A 2012;421-422(0):99–107.
[17] Xu QC, Lin JD, Li J, Fu XZ, Liang Y, Liao DW. Microwave-assisted synthesis of MgO–CNTs supported ruthenium catalysts for ammonia synthesis. Catal Commun 2007;8(12):1881–5.
[18] Shan B, Cho K. First-principles study of work functions of double-wall carbon nanotubes. Phys Rev B 2006;73(8):081401.
[19] Chen W, Fan Z, Pan X, Bao X. Effect of confinement in carbon nanotubes on the activity of Fischer-Tropsch iron catalyst. J Am Chem Soc 2008;130(29):9414–9.
[20] Abbaslou RMM, Tavassoli A, Soltan J, Dalai AK. Iron catalysts supported on carbon nanotubes for Fischer–Tropsch synthesis: Effect of catalytic site position. Appl Catal A 2009;367:47–52.
[21] Surisetty VR, Tavasoli A, Dalai AK. Synthesis of Higher alcohols from syngas over alkali promoted MoS2 catalysts supported on muti-walled carbon nanotubes. Appl Catal A 2009;365:243–51.
[22] Yang QH, Hou PX, Bai S, Wang MZ, Cheng HM. Adsorption and capillarity of nitrogen in aggregated multi-walled carbon nanotubes. Chem Phys Lett 2001;345(1–2):18–2424.
[23] Wu H, Wexler D, Ranjbartoreh AR, Liu H, Wang G. Chemical processing of double-walled carbon nanotubes for enhanced hydrogen storage. Int J Hydrogen Energy 2010;35(12):6345–9.
[24] Song S, Yang H, Rao R, Liu H, Zhang A. Defects of multi-walled carbon nanotubes as active sites for benzene hydroxylation to phenol in the presence of H_2O_2. Catal Commun 2010;11(8):783–7.
[25] Dresselhaus MS, Dresselhaus G, Saito R, Jorio A. Raman spectroscopy of carbon nanotubes. Phys Reports 2005;40:47–99.
[26] Costa S, Borowiak-Palen E, Kruszynska M, Bachmatiuk A, Kalenczuk RJ. Characterization of carbon nanotubes by Raman spectroscopy. Mater Sci-Poland 2008;26:433–41.
[27] Yang H, Song S, Rao R, Wang X, Yu Q, Zhang A. Enhanced catalytic activity of benzene hydrogenation over nickel confined in carbon nanotubes. J Mol Catal A 2010;323(1–2):33–9.